AAS 15-616

RAPID GENERATION OF OPTIMAL ASTEROID POWERED DESCENT TRAJECTORIES VIA CONVEX OPTIMIZATION

Robin Pinson* **and Ping Lu†**

This paper investigates a convex optimization based method that can rapidly generate the fuel optimal asteroid powered descent trajectory. The ultimate goal is to autonomously design the optimal powered descent trajectory on-board the spacecraft immediately prior to the descent burn. Compared to a planetary powered landing problem, the major difficulty is the complex gravity field near the surface of an asteroid that cannot be approximated by a constant gravity field. This paper uses relaxation techniques and a successive solution process that seeks the solution to the original nonlinear, nonconvex problem through the solutions to a sequence of convex optimal control problems.

INTRODUCTION

Mission proposals that land spacecraft on asteroids are becoming increasingly popular. However, in order to have a successful mission the spacecraft must reliably and softly land at the intended landing site with pin-point precision. The problem under investigation is how to design a fuel optimal powered descent trajectory that can be quickly computed on-board the spacecraft, without interaction from ground control. An optimal trajectory designed immediately prior to the powered descent burn has many advantages. These advantages include the ability to use the actual vehicle starting state as the initial condition in the trajectory design and the ease of updating the target landing site. For long trajectories, the trajectory can be updated periodically by a redesign of the optimal trajectory based on current vehicle conditions to improve guidance performance. One of the key drivers for being completely autonomous is the infrequent and delayed communication between ground control and the vehicle. Challenges that arise from designing an asteroid powered descent trajectory include complicated nonlinear gravity fields, small rotating bodies and low thrust vehicles. There are many factors that will not be understood until the spacecraft reaches the asteroid, which is why many missions spend long periods of time near the asteroid characterizing it and choosing the landing site. It is imperative to make the trajectory design algorithm as flexible as possible to account for this new information.

There have been two successful landings on asteroids and one on a comet over the last two decades. NEAR was the first successful landing. NASA decided to attempt a controlled descent, after debating options for the spacecraft following completion of the primary mission objectives. The NEAR spacecraft was not designed to land on Eros, which led to designing landing operations after launch. Four braking maneuvers were planned over a 50 minute period. Each maneuver targeted a specified decrease in vehicle velocity. It was expected that the vehicle would impact the surface with a 1.3 m/s velocity. The spacecraft impacted earlier than expected in the range of 1.5-1.8 m/s.[1] Due to malfunctioning equipment, Hayabusa was painstakingly guided to a point near the landing site from ground control, even with a 20 minute communication delay. Close to the surface, landing target markers were dropped to the surface and Hayabusa rendezvoused with the markers to successfully reach the surface.[2] Rosetta's lander Philae followed a ballistic trajectory down to the comet's surface. When the trajectory was originally analyzed there were two options, a completely passive trajectory and an option containing one pre-planned maneuver.[3,4]

There are a handful of proposed missions to asteroids whose landing algorithms and missions are still being finalized. Most rely on ballistic trajectories or ground designed trajectories and waypoints. The lander

*Aerospace Engineer, Guidance, Navigation and Mission Analysis Branch, NASA MSFC, EV42, MSFC, AL 35812.
†Professor, Department of Aerospace Engineering, Iowa State University, Ames, IA 50011

MASCOT relies on the primary spacecraft to drop down to 100 m altitude and then MASCOT free falls to the surface for the Marco Polo and Hayabusa-2 missions.[5,6] OSIRIS-REx has a checkpoint and a matchpoint at which maneuvers will be performed. These are targeted maneuvers which are adjusted on-board to account for differences between the originally designed points and the actual spacecraft conditions at those points. The last maneuver at the matchpoint is eight minutes prior to touchdown at 45 m altitude and slows the descent velocity.[7]

Since the asteroid powered descent trajectory design is a new field of study, there are a wide range of proposed methods and ideas that are being developed. All of these ideas have advantages and disadvantages. The trajectory design and related guidance algorithms are both studied, as some methods forgo trajectory design and focus entirely on closed loop guidance efforts. One proposed approach to the rapid generation of the descent trajectory is a semi-analytical approach which assumes the acceleration profile is a cubic polynomial. Given the acceleration profile shape with known initial and final points, the problem is solved analytically except for three parameters: time of flight, initial thrust and initial thrust angle. Combining these with path constraints yields a nonlinear program which is then solved. This method does allow for rapidly designing a trajectory at the cost of a non-optimal solution due to the acceleration assumption.[8] A second approach for designing the descent trajectory focuses on extracting information from the optimal control theory formulation of the problem. An indirect method that propagates and solves the costates, boundary conditions and differential equations is combined with a direct method that optimizes the original cost function. This combination decreases the computation time as compared to directly optimizing the nonlinear cost function and original problem formulation.[9]

Variations on sliding mode control theory as a guidance algorithm for the descent trajectory is found in several places. Sliding mode control theory is a robust control law when faced with bounded disturbances. One method uses multiple sliding surfaces to drive the spacecraft to the landing site in a finite amount of time.[10] Other proposals use a predesigned trajectory and apply variations on sliding mode control theory to counteract disturbances while tracking the trajectory.[11,12] One proposed method of predesigning the trajectory is to apply a homotopic and successive solution technique while solving the state and costate differential equations via a shootout method.[12]

There are two previous studies that form the background to the current investigation. The first study looked in-depth at applying convex optimization to a powered descent trajectory on Mars with promising results.[13] This showed that the powered descent equations of motion can be relaxed and formed into a convex optimization problem and that the optimal solution of the relaxed problem is indeed a feasible solution to the original problem. This analysis used a constant gravity field, which is a poor approximation for an asteroid. In addition, these authors have looked into including thrust pointing constraints, while achieving lossless convexification.[14] The second study applied a successive solution process to formulate a second order cone problem that designs rendezvous and proximity operations trajectories.[15] These trajectories included a Newtonian gravity model. The equivalence of the solutions between the relaxed and the original problem was theoretically established.

Convex optimization had great success in the above studies and the focus of this analysis is the applicability to the asteroid powered descent problem. A key advantage of using convex optimization and its subclasses is that as long as there is at least one feasible solution, the global minimum is guaranteed in a finite number of steps. A wide range of functions and formulations are included in the convex variable class and convex optimization including second order cone programming and linear programming.

The fuel optimal control problem in this work is to determine the optimal (finite) thrust vector (both magnitude and direction) to land the spacecraft at a specified location, in the presence of a highly nonlinear gravity field and subject to various mission and operational constraints. The proposed solution is to use convex optimization, a gravity model with higher fidelity than Newtonian, and an iterative solution process to design the fuel optimal trajectory. The solution to the convex optimization problem is the thrust profile, magnitude and direction, that will yield the minimum fuel trajectory for a soft landing at the target site.

This paper discusses the optimization problem formulation and spacecraft dynamics, including the gravity model. The original formulation is not in a convex optimization format. The steps and methods taken to

generate the problem into a convex form that will yield the same optimal solution as the original problem is the main focus. Relaxation techniques, investigation into problem equivalence, change of variables and a successive solution method are all used to generate the final optimization problem that can be solved with a convex optimizer. Following this discussion will be results and trends seen from generating trajectories with this process.

ORIGINAL PROBLEM FORMULATION

For a soft landing on an asteroid, the trajectory is designed as a two point boundary value problem. The state of the spacecraft at the start of the powered descent burn is known, along with the landing site location. A soft landing occurs when the spacecraft has zero velocity relative to the landing site.

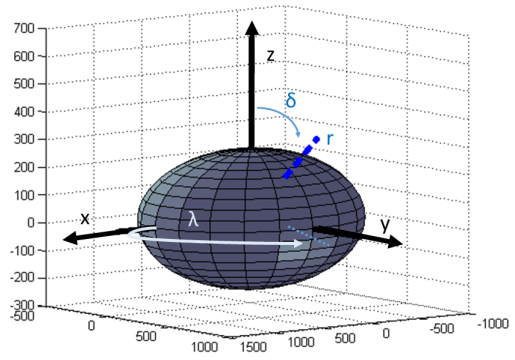

Figure 1. Asteroid centered fixed coordinate system example. Scale is in meters.

The dynamics of the landing trajectory and the corresponding equations of motion are formulated in an asteroid centered fixed (ACF) Cartesian coordinate system. This coordinate system, depicted in Figure 1, is fixed at the asteroid's center of mass. The x axis is aligned with the largest semi-major axis (minimum moment of inertia), the z axis is aligned with the smallest semi-major axis (maximum moment of inertia) and the y axis is aligned with the intermediate semi-major axis. For asteroids that are not perfect ellipsoids, the axes are as closely aligned as possible, while still keeping an orthogonal coordinate system. The majority of the work will be in the Cartesian coordinate system; however, some models are originally derived in spherical coordinates and then transformed into Cartesian coordinates. The variable r is the radius from the center of the asteroid to the spacecraft. The two angles are latitude (δ) measured from the z axis to the radius vector and longitude (λ) measured from the x axis to the projection of the radius in the x-y plane.

The ACF is a rotating frame around the asteroid's spin axis $\vec{\omega}$ with a spin rate of ω. In order to apply the dynamic equations to all asteroids, including those with a rotation axis not aligned with the z axis or tumbling asteroids, the spin axis is allowed to be a time-varying vector. The equations of motion of the spacecraft include the rotational effects of the coordinate system, Eq. (1).

$$\vec{T} + m\nabla U = m\left(\frac{d\vec{v}}{dt} + 2\vec{\omega}\times\vec{v} + \dot{\vec{\omega}}\times\vec{r} + \vec{\omega}\times(\vec{\omega}\times\vec{r})\right) \tag{1}$$

The position and velocity vectors of the spacecraft in the ACF frame are represented by $\vec{r}$ and $\vec{v}$. The vehicle thrust vector is $\vec{T}$ and the acceleration due to gravity is the gradient of the gravitational potential (∇U).

The gravitational potential (U) is a function of spacecraft position for all the gravity models: Newtonian, spherical potential, polyhedron and interior spherical potential. For this paper, the spherical potential function for a triaxial ellipsoid will be used as the gravitational potential. The standard form of the spherical potential is given in Eq. (2).[16]

$$U = \frac{\mu}{r}\sum_{l=0}^{\infty}\sum_{m=0}^{l}\left(\frac{r_o}{r}\right)^l P_{l,m}\left[\sin\delta\right]\left\{C_{l,m}\cos\left(m\lambda\right) + S_{l,m}\sin\left(m\lambda\right)\right\} \tag{2}$$

In the model located in Eq. (2), the gravitational potential is based on the distance from the center of mass or radius (r), the latitude (δ) and the longitude (λ) of the spacecraft. The coefficients $C_{l,m}$ and $S_{l,m}$ are unique to the asteroid. These coefficients can be determined in a number of ways. The reference radius (r_o) is associated with the coefficients, usually taken to be the maximum radius of the asteroid. The gravitational constant is represented by μ and $P_{l,m}$ is the associated Legendre function. While the potential function is an infinite sum in order to represent the effects of the mass over the entire body shape, the summation can be truncated and still yield reasonable accuracy. The desired accuracy dictates the order and degree of the model that is used. A good initial model for an asteroid is to use a 2x2 model, and assume the asteroid is a homogenous (constant density) triaxial ellipsoid.[17] For this case, the upper limits on the summation are both 2. Due to the fact that the origin of the ACF coordinate system is at the center of mass and the symmetry of the homogenous ellipsoid, only $C_{0,0}$, $C_{2,0}$ and $C_{2,2}$ are nonzero. By definition $C_{0,0} = 1$. The gravitational potential for the triaxial ellipsoid reduces to Eq. (3).

$$U = \frac{\mu}{r}\left\{1 + \left(\frac{r_o}{r}\right)^2\left[C_{2,0}\left(\frac{3}{2}\sin^2\delta - \frac{1}{2}\right) + C_{2,2}\left(3\cos^2\delta\right)\cos\left(2\lambda\right)\right]\right\} \tag{3}$$

The acceleration components due to gravity or the gradient of the gravitational potential in the ACF Cartesian coordinate system are given in Eq. (4).

$$\begin{aligned}
\frac{\partial U}{\partial r_x} =& -\frac{\mu}{r^3}r_x + -\frac{\mu}{r^3}\left(G_1 r_x + G_2\frac{r_x r_z}{\left(r_x^2 + r_y^2\right)^{0.5}}\right) + \frac{\mu}{r}G_3 r_y \\
\frac{\partial U}{\partial r_y} =& -\frac{\mu}{r^3}r_y + -\frac{\mu}{r^3}\left(G_1 r_y + G_2\frac{r_y r_z}{\left(r_x^2 + r_y^2\right)^{0.5}}\right) - \frac{\mu}{r}G_3 r_x \\
\frac{\partial U}{\partial r_z} =& -\frac{\mu}{r^3}r_z + -\frac{\mu}{r^3}\left(G_1 r_z + G_2\frac{r_z^2}{\left(r_x^2 + r_y^2\right)^{0.5}}\right) + \frac{\mu}{r}\frac{G_2}{\left(r_x^2 + r_y^2\right)^{0.5}}
\end{aligned} \tag{4}$$

The terms G_1, G_2 and G_3 are defined in Eq. (5).

$$\begin{aligned}
G_1 =& \frac{r_o^2}{r^2}\left\{3C_{2,0}\left[1.5sin^2\left(\delta\right) - 0.5\right] + 9C_{2,2}cos^2\left(\delta\right)cos\left(2\lambda\right)\right\} \\
G_2 =& \frac{r_o^2}{r^2}\left\{1.5C_{2,0}sin\left(2\delta\right) - 3C_{2,2}sin\left(2\delta\right)cos\left(2\lambda\right)\right\} \\
G_3 =& \frac{r_o^2}{r^2}\left\{\frac{1}{\left(r_x^2 + r_y^2\right)}6C_{2,2}cos^2\left(\delta\right)sin\left(2\lambda\right)\right\}
\end{aligned} \tag{5}$$

The gradient in Eq. (4) is highly nonlinear in the position vector, including radius raised to the fifth power and cross products of position components. When $C_{2,0}$ and $C_{2,2}$ are zero, Eq. (4) reduces to the standard Newtonian field with $\frac{\partial U}{\partial \vec{r}} = -\frac{\mu}{r^3}\vec{r}$.

The problem's optimization objective is minimization of the fuel usage (or propellant usage), while still landing softly. This is achieved by maximizing the mass of the vehicle when it touches down, thus minimizing fuel consumption for the given initial mass. To accomplish this, the minimization cost function (Eq. (6)) is the negative of the mass at the landing site. The full optimization problem is stated in Eq. (6) through Eq. (18),

referred to as Problem P1. The states are $\vec{r},\ \vec{v},\ m$ and the control vector is $\vec{T}$.

$$\min -m(t_f) \tag{6}$$

$$s.t.\ \dot{\vec{r}} = \vec{v} \tag{7}$$

$$\dot{\vec{v}} = \frac{\vec{T}}{m} - 2\vec{\omega} \times \vec{v} - \dot{\vec{\omega}} \times \vec{r} - \vec{\omega} \times (\vec{\omega} \times \vec{r}) + \nabla U(\vec{r}) \tag{8}$$

$$\dot{m} = -\frac{1}{v_{ex}} \left\| \vec{T} \right\| \tag{9}$$

$$T_{min} \leq \left\| \vec{T} \right\| \leq T_{max} \tag{10}$$

$$\|\vec{r}\| cos\theta - \vec{r}^{\,T} \hat{n} \leq 0 \tag{11}$$

$$m \geq m_{dry} \tag{12}$$

$$\vec{r}\,(0) = \vec{r}_0 \tag{13}$$

$$\vec{v}\,(0) = \vec{v}_0 \tag{14}$$

$$m\,(0) = m_{wet} \tag{15}$$

$$\vec{r}\,(t_f) = \vec{r}_f \tag{16}$$

$$\vec{v}\,(t_f) = \vec{v}_f \tag{17}$$

$$t_f \ \text{ given} \tag{18}$$

Initial conditions, position ($\vec{r}_0$), velocity ($\vec{v}_0$) and total spacecraft mass including propellant (m_{wet}), are known, Eq. (13), Eq. (14) and Eq. (15). This is a fixed final time (t_f) problem with t_f specified. The final position ($\vec{r}_f$) and velocity ($\vec{v}_f$) are based on the landing site, Eq. (16) and Eq. (17). In the problem formulation, once the engine has been turned on, it is assumed to be throttleable between a minimum and maximum magnitude (T_{min} and T_{max}) with $T_{min} > 0$, because the engine cannot be turned off until the descent burn is complete. This is accounted for by inequality constraints on the thrust magnitude, Eq. (10). The associated exit velocity (v_{ex}) is the product of the vehicle Isp and reference gravity at Earth sea level. The final mass is free, as long as the vehicle does not use more than the allowable propellant which is protected for by the constraint in Eq. (12). When the vehicle mass reaches the vehicle dry mass, m_{dry}, all propellant has been consumed.

The above optimal control problem is nonlinear and nonconvex. The presence of the thrust vector norm in Eq. (9) and Eq. (10) and the mass in the denominator of Eq. (8) cause those equations to be nonlinear. The gravitational acceleration in Eq. (8) is highly nonlinear in the position vector. The thrust constraint Eq. (10) can be divided into two constraints.

$$\begin{aligned} T_{min} &\leq \left\| \vec{T} \right\| \\ \left\| \vec{T} \right\| &\leq T_{max} \end{aligned} \tag{19}$$

The second inequality in Eq. (19) is convex and an allowable inequality for a convex optimization problem, while the first inequality is not. Therefore, to solve this problem by convex optimization, which requires equality constraints to be linear and inequality constraints to be convex, the nonlinearities in this problem will need to be handled with a variety of techniques.

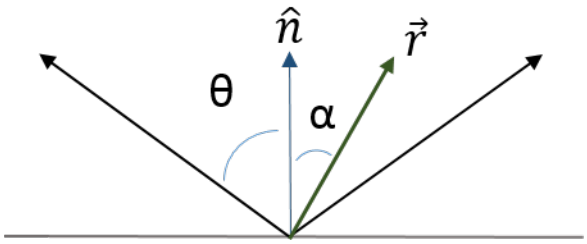

Figure 2. Illustration of glide slope constraint.

The constraint in Eq. (11) is a glide slope constraint, which represents an approach cone surrounding the landing site. The cone is defined by the angle θ, which is limited to $0 \leq \theta \leq 90$ deg. When θ is 90 deg, this ensures that the vehicle altitude is always positive and the trajectory design does not try to fly below the surface before reaching the landing site. The unit vector normal to the asteroid surface at the landing site is $\hat{n}$. The angle between the spacecraft position vector and the landing site normal is α, which the constraint ensures to be less than or equal to θ.

CONVEXIFICATION AND RELAXATION OF THE PROBLEM

The magnitude of the thrust vector or norm of the thrust vector is one of the nonlinearities in the original problem. In order to remove nonlinearities, a slack variable T_m will be added to become a fourth control to supplement $\vec{T}$. In the relaxed optimal control problem, this variable is completely separate from the thrust vector and only related through a new constraint, Eq. (20).

$$\left\|\vec{T}\right\| \leq T_m \tag{20}$$

This slack variable T_m replaces the magnitude of the thrust vector in Problem P1. The new optimal control problem, now called Problem P2, is defined in Eq. (21) through Eq. (33).

$$\min -m(t_f) \tag{21}$$

$$s.t.\ \ \dot{\vec{r}} = \vec{v} \tag{22}$$

$$\dot{\vec{v}} = \frac{\vec{T}}{m} - 2\vec{\omega} \times \vec{v} - \dot{\vec{\omega}} \times \vec{r} - \vec{\omega} \times (\vec{\omega} \times \vec{r}) + \nabla U(\vec{r}) \tag{23}$$

$$\dot{m} = -\frac{1}{v_{ex}} T_m \tag{24}$$

$$\left\|\vec{T}\right\| \leq T_m \tag{25}$$

$$T_{min} \leq T_m \leq T_{max} \tag{26}$$

$$m \geq m_{dry} \tag{27}$$

$$\vec{r}\,(0) = \vec{r}_0 \tag{28}$$

$$\vec{v}\,(0) = \vec{v}_0 \tag{29}$$

$$m\,(0) = m_{wet} \tag{30}$$

$$\vec{r}\,(t_f) = \vec{r}_f \tag{31}$$

$$\vec{v}\,(t_f) = \vec{v}_f \tag{32}$$

$$t_f \ \text{ given} \tag{33}$$

With the introduction of the slack variable T_m Eq. (24) and Eq. (26) are now linear and the constraint in Eq. (25) is convex. The remaining nonlinearities are the first and last terms on the right hand side of Eq. (23).

The glide slope constraint in Eq. (11) is not included in Problem P2 for brevity of the discussion below. Correspondingly, it is understood that the glide slope constraint has also been removed from Problem P1 in the following discussion.

As Problem P2 will be solved in this paper, an immediate question arises as to the relationship between the solutions to Problems P1 and P2. To answer this critical question, examine the following results.

Proposition 1: Problems P1 and P2 are identical when the inequality in Eq. (25) is active, i.e., $\left\|\vec{T}\right\| = T_m$. Moreover, the solution to Problem P2 is the same as the solution to Problem P1.

Proof: The first part of Proposition 1 is straightforward. It is immediately clear that when the constraint in Eq. (27) is active, Problem P2 reduces to Problem P1. To prove the second part of the Proposition, apply the Minimum Principle from optimal control theory[18] and form the Hamiltonian in a vector and matrix format that removes the cross products, Eq. (34). Note that the cost function is only dependent on the mass at the final time, $\phi\left(t_f\right) = -m(t_f)$. The dynamics of the system are autonomous causing the Hamiltonian to be constant during the entire flight.

$$\begin{gathered} H = \vec{p}_r^{\,T}\vec{v} + \vec{p}_v^{\,T}\left(\tfrac{1}{m}\vec{T} - 2W_1\vec{v} - W_2\vec{r} - W_3\vec{r} + \nabla U\left(\vec{r}\right)\right) - p_m\tfrac{1}{v_{ex}}T_m \\ W_1 = \begin{bmatrix} 0 & -\omega_z & \omega_y \\ \omega_z & 0 & -\omega_x \\ -\omega_y & \omega_x & 0 \end{bmatrix} \quad W_2 = \begin{bmatrix} 0 & -\dot{\omega}_z & \dot{\omega}_y \\ \dot{\omega}_z & 0 & -\dot{\omega}_x \\ -\dot{\omega}_y & \dot{\omega}_x & 0 \end{bmatrix} \\ W_3 = \begin{bmatrix} -\omega_y^2 - \omega_z^2 & \omega_x\omega_y & \omega_x\omega_z \\ \omega_x\omega_y & -\omega_x^2 - \omega_z^2 & \omega_y\omega_z \\ \omega_x\omega_z & \omega_y\omega_z & -\omega_x^2 - \omega_y^2 \end{bmatrix} \end{gathered} \tag{34}$$

The states are $\vec{r}$, $\vec{v}$, m, and the corresponding costates are $\vec{p}_r$, $\vec{p}_v$, p_m. The control vector $\mathscr{C}$ consists of the thrust vector and slack variable and the constraints on the control vector are described in Eq. (35).

$$\mathscr{C} = \left\{\left(\vec{T}, T_m\right) \mid \left\|\vec{T}\right\| \leq T_m,\, T_{min} \leq T_m,\, T_m \leq T_{max}\right\} \tag{35}$$

From optimal control theory, the differential equations for the costates are listed in Eq. (36) through Eq. (38).

$$\dot{\vec{p}}_r = W_2^T\vec{p}_v + W_3^T\vec{p}_v - \vec{p}_v^{\,T}\nabla^2 U(\vec{r}) \tag{36}$$

$$\dot{\vec{p}}_v = -\vec{p}_r + 2W_1^T\vec{p}_v \tag{37}$$

$$\dot{p}_m = \vec{p}_v^{\,T}\vec{T}\left(\frac{1}{m^2}\right) \tag{38}$$

The problem is a fixed final time problem. Applying the end point constraints and the transversality conditions yields one useful equation, Eq. (39).

$$p_m\left(t_f\right) = -1 \tag{39}$$

From the Minimum Principle, the optimal solution is determined by minimizing the Hamiltonian with respect to the control vector ($\mathscr{C}$) subject to the constraints in Eq. (35). The Hamiltonian is linear in terms of the control vector, therefore the minimum will be on the boundary of the admissible control set. This can be turned into a constrained optimization problem which minimizes the Hamiltonian by applying the Kasrush-Kuhn-Tucker (KKT) conditions. First, the terms in the Hamiltonian expression that are not dependent on the control vector can be removed from the optimization problem, as they have no effect on the solution. These terms are $\vec{p}_r^{\,T}\vec{v} + \vec{p}_v^{\,T}\left(-2W_1\vec{v} - W_2\vec{r} - W_3\vec{r} + \nabla U\left(\vec{r}\right)\right)$. It is interesting to note that as long as the gravitational potential remains a function of spacecraft position, it does not influence the minimization of the Hamiltonian. Increasing the complexity of the gravity model will not invalidate these arguments.

The point-wise minimization problem with respect to $\vec{T},\ T_m$ is stated in Eq. (40).

$$\begin{gathered} \min\ \tfrac{1}{m}\vec{p}_v^{\,T}\vec{T} - \tfrac{1}{v_{ex}}p_m T_m \\ s.t.\ \left\|\vec{T}\right\| \leq T_m,\, T_{min} \leq T_m,\, T_m \leq T_{max} \end{gathered} \tag{40}$$

This is a convex optimization problem which has a global optimal solution. The Lagrangian for the constrained optimization problem is listed in Eq. (41).

$$\mathscr{L} = \frac{1}{m}\vec{p}_v^{\,T}\vec{T} - \frac{1}{v_{ex}}p_m T_m + \lambda_1\left(\left\|\vec{T}\right\| - T_m\right) + \lambda_2\left(T_{min} - T_m\right) + \lambda_3\left(T_m - T_{max}\right) \tag{41}$$

The variables $\lambda_1,\ \lambda_2,\ \lambda_3$ are the Lagrange multipliers associated with the inequality constraints on $\vec{T},\ T_m$. From the KKT conditions, a constraint is active when $\lambda_i \geq 0$, while a constraint can only be inactive when $\lambda_i = 0$. Applying the KKT conditions yields Eq. (42) and Eq. (43).

$$\frac{\partial \mathscr{L}}{\partial \vec{T}} = \frac{1}{m}\vec{p}_v + \lambda_1\frac{\vec{T}}{\left\|\vec{T}\right\|} = 0 \tag{42}$$

$$\frac{\partial \mathscr{L}}{\partial T_m} = -\frac{1}{v_{ex}}p_m - \lambda_1 - \lambda_2 + \lambda_3 = 0 \tag{43}$$

Now examine the problem as two specific cases when $\vec{p}_v$ is nonzero almost everywhere (a.e.) in $[0, t_f]$ and when it is zero in a finite time interval. For the first case it will be shown that $\lambda_1 \neq 0$, therefore the solutions to Problems P1 and P2 are the same. Then by contradiction, show that $\vec{p}_v$ cannot be zero in a finite time interval.

Suppose that $\vec{p}_v \neq 0$ in any finite time interval. From Eq. (42), when $\vec{T} \neq 0$, then λ_1 must be nonzero ($\lambda_1 \neq 0$); otherwise, Eq. (42) necessitates $\vec{p_v} = 0$, since mass is nonzero, contradicting the assumption that $\vec{p}_v \neq 0$. When $\vec{T} = 0$, $\vec{T}/||\vec{T}||$ is a finite vector. The same argument applies to ascertain that $\lambda_1 \neq 0$. Therefore, the corresponding constraint must be active, $\left\|\vec{T}\right\| = T_m$. Consequently, the solution to Problem P2 is also the solution to Problem P1.

Next look at the case when $\vec{p}_v = 0$ for a finite time period. If $\vec{p}_v = 0$ in a finite time interval, its derivative must also be zero simultaneously. From the costate equations in Eq. (36) through Eq. (38), this implies that $\vec{p}_r = 0$ and p_m is a constant. Because the costate system in Eq. (36) through Eq. (38) is a homogeneous linear system in $\vec{p}_r$ and $\vec{p}_v$, it follows that $\vec{p}_r = \vec{p}_v = 0$ in the entire interval $[0, t_f]$, and p_m is constant. From the transversality condition in Eq. (39), $p_m(t) = -1$. The Hamiltonian reduces to Eq. (44).

$$H = \frac{1}{v_{ex}}T_m \tag{44}$$

The minimum of the Hamiltonian with respect to $\mathscr{C}$ is the smallest admissible T_m, which is $T_{min} > 0$, therefore $T_m = T_{min}$. Thus the Hamiltonian becomes Eq. (45).

$$H = \frac{1}{v_{ex}}T_{min} \tag{45}$$

If $\vec{p}_v = 0$ in a finite interval, the constancy condition of the Hamiltonian, Eq. (45), should always hold, regardless of the initial conditions, landing site, or the specified final time t_f. In particular, if the value of t_f happens to be equal to t_f^*, the optimal flight time in a free-time problem, which is the same as Problem P2 except that the final time is free, the Hamiltonian is zero along the optimal trajectory from the Minimum Principle. The nonzero constancy condition in Eq. (45) then constitutes a contradiction in this case. Therefore, the condition that $\vec{p}_v = 0$ in a finite interval cannot happen. Since this case is invalid, the case of $\vec{p}_v \neq 0$ a.e. on $[0, t_f]$ is the only possibility, which in turn means that $\left\|\vec{T}\right\| = T_m$ in the solution to Problem P2. This solution is also the solution to Problem P1.

CHANGE OF VARIABLES

The next step of the process that turns Problems P1 and P2 into a convex optimization problem is a change of variable for two variable types. The first changes the thrust variables into acceleration due to thrust with

the conversion seen in Eq. (46).

$$\begin{aligned} \vec{a}_t = &\quad \frac{\vec{T}}{m} \\ a_{tm} = &\quad \frac{T_m}{m} \end{aligned} \tag{46}$$

In addition, a new mass variable and its derivative are introduced to replace the current mass variables. This transformation is seen in Eq. (47).

$$\begin{aligned} q &= ln\left(m\right) \\ \dot{q} &= -\frac{a_{tm}}{v_{ex}} \end{aligned} \tag{47}$$

This change affects the cost function. The properties of the natural log function allow maximum mass to correspond to the maximum of q.

After the change of variables, the constraint in Eq. (26) becomes the two inequality expressions in Eq. (48).

$$\begin{aligned} T_{min}\mathrm{e}^{-q} &\leq a_{tm} \\ a_{tm} &\leq T_{max}\mathrm{e}^{-q} \end{aligned} \tag{48}$$

Taylor's series expansion will be applied to e^{-q}, in order to turn the top inequality into a quadratic equation in state and the bottom into a linear. This effectively creates a second order cone constraint and a linear constraint, which are both convex. A quadratic cannot be used on the bottom constraint as that would not yield a convex constraint. The new constraints (Eq. (49)) are equivalent to the old as long as the expansion does not deviate from the original mass. Spot checking shows the difference is on the order of a few grams, which is negligible to ensuring the thrust bounds are not exceeded.

$$\begin{aligned} T_{min}\mathrm{e}^{-q_o}\left[1-\left(q-q_o\right)+0.5\left(q-q_o\right)^2\right] &\leq a_{tm} \\ a_{tm} &\leq T_{max}\mathrm{e}^{-q_o}\left[1-\left(q-q_o\right)\right] \end{aligned} \tag{49}$$

The point about which the expansion occurs (q_o) is calculated ahead of time. It is vehicle mass profile assuming the vehicle has been running at minimum thrust for the entire flight, Eq. (50).

$$q_o = \ln\left(m_{wet} - \frac{T_{min}}{v_{ex}}\triangle t\right) \tag{50}$$

In the above equation, Δt is the time elapsed from the start of the burn.

After the change in variables and Taylor series expansion, the optimization problem becomes Problem P3

found in Eq. (51) through Eq. (64).

$$\min -q(t_f) \tag{51}$$

$$s.t.\ \dot{\vec{r}} = \vec{v} \tag{52}$$

$$\dot{\vec{v}} = \vec{a}_t - 2\vec{\omega} \times \vec{v} - \dot{\vec{\omega}} \times \vec{r} - \vec{\omega} \times (\vec{\omega} \times \vec{r}) + \nabla U(\vec{r}) \tag{53}$$

$$\dot{q} = -\frac{1}{v_{ex}} a_{tm} \tag{54}$$

$$\|\vec{a}_t\| \leq a_{tm} \tag{55}$$

$$T_{min} \mathrm{e}^{-q_o} \left[1 - (q - q_o) + 0.5\,(q - q_o)^2\right] \leq a_{tm} \tag{56}$$

$$a_{tm} \leq T_{max} \mathrm{e}^{-q_o} \left[1 - (q - q_o)\right] \tag{57}$$

$$q \geq q_{dry} \tag{58}$$

$$\vec{r}\,(0) = \vec{r}_0 \tag{59}$$

$$\vec{v}\,(0) = \vec{v}_0 \tag{60}$$

$$q\,(0) = \ln\left(m_{wet}\right) \tag{61}$$

$$\vec{r}\,(t_f) = \vec{r}_f \tag{62}$$

$$\vec{v}\,(t_f) = \vec{v}_f \tag{63}$$

$$t_f \ \text{ given} \tag{64}$$

Problem P3 is equivalent to Problem P2 as long as the Taylor series expansion is a good approximation. The optimal solution for Problem P3 is the optimal solution of Problem P2 and thus Problem P1. With the exception of the gravitational acceleration, the dynamics are linear in state and control, while the inequality constraints are linear or second order cones, yielding a convex optimization problem. The gravitational acceleration nonlinear term will be handled via a successive solution method.

SUCCESSIVE SOLUTION METHOD

The gravitational acceleration is the most challenging aspect to manipulate into a convex form. Recall that the 2x2 triaxial ellipsoid gravitational acceleration is highly nonlinear in the position vector including radius raised to the fifth power and cross multiplication of position terms. The best way to handle these nonlinearities is to introduce a successive solution method. In the successive solution method a series of convex optimization problems are solved with each one using data from the previous solution, also known as iterations. The equations of motion from Problem P3, found in Eq. (52) through Eq. (54), can be rearranged into Eq. (65), where (k) is the current iteration and (k-1) is the previous iteration.

$$\dot{\vec{x}}^{(k)} = A\left(r^{(k-1)}\right)\vec{x}^{(k)} + B\vec{u}^{(k)} + c\left(r^{(k-1)}\right) \tag{65}$$

The full state is represented by $\vec{x} = \left[\vec{r}^{\,T},\, \vec{v}^{\,T},\, q\right]^T$ and the control vector $\vec{u} = \left[\vec{a}_t^{\,T},\, a_{tm}\right]^T$. The B matrix is constant throughout the flight and between iterations. The terms from the gravitational acceleration are divided between the A matrix and c vector and evaluated with the previous iteration's solution. Five different arrangements of the terms in A and c were tried. The best one placed the Newtonian terms in the A matrix and all the remaining terms in the c vector, see Eq. (66). Thus, c can be thought of as a vector of higher order terms. With this arrangement it should be simple to swap out the 2x2 triaxial model for a higher fidelity

model.

$$A = \begin{bmatrix} 0 & 0 & 0 & 1 & 0 & 0 & 0 \\ 0 & 0 & 0 & 0 & 1 & 0 & 0 \\ 0 & 0 & 0 & 0 & 0 & 1 & 0 \\ \omega^2 - \frac{\mu}{r^3} & 0 & 0 & 0 & 2\omega & 0 & 0 \\ 0 & \omega^2 - \frac{\mu}{r^3} & 0 & -2\omega & 0 & 0 & 0 \\ 0 & 0 & -\frac{\mu}{r^3} & 0 & 0 & 0 & 0 \\ 0 & 0 & 0 & 0 & 0 & 0 & 0 \end{bmatrix}^{(k-1)} \qquad B = \begin{bmatrix} 0 & 0 & 0 & 0 \\ 0 & 0 & 0 & 0 \\ 0 & 0 & 0 & 0 \\ 1 & 0 & 0 & 0 \\ 0 & 1 & 0 & 0 \\ 0 & 0 & 1 & 0 \\ 0 & 0 & 0 & -\frac{1}{v_{ex}} \end{bmatrix}$$

$$c = \begin{bmatrix} 0 \\ 0 \\ 0 \\ -\frac{\mu}{r^3}\left(G_1 r_x + G_2 \frac{r_x r_z}{\sqrt{\left(r_x^2 + r_y^2\right)}}\right) + \frac{\mu}{r} G_3 r_y \\ -\frac{\mu}{r^3}\left(G_1 r_y + G_2 \frac{r_y r_z}{\sqrt{\left(r_x^2 + r_y^2\right)}}\right) - \frac{\mu}{r} G_3 r_x \\ -\frac{\mu}{r^3}\left(G_1 r_z + G_2 \frac{r_z^2}{\sqrt{\left(r_x^2 + r_y^2\right)}}\right) + \frac{\mu}{r} \frac{1}{\sqrt{\left(x_k^2 + y_k^2\right)}} G_2 \\ 0 \end{bmatrix}^{(k-1)} \tag{66}$$

A and c are functions of position, since the nonlinear terms in the gravitational acceleration are position. For the first iteration the position vector is taken to be the initial condition for the entire trajectory, equivalent to assuming the spacecraft hovered at the initial point for the entire length of trajectory. Iterations continue until the current iteration and previous iteration match within a specified tolerance. At this point they are close enough to be called equivalent and the gravitational acceleration used to develop the current trajectory is no longer an approximation.

By using the previous trajectory to evaluate the gravitational acceleration, the dynamics are now linear and thus the problem is a convex optimization problem. Actually, it is in a second order cone program format, which is a subset of convex optimization. In order to keep the problem generic and allow for additional constraints or dynamics, a convex optimizer will be used. A second order cone program is also an option for solving the problem in its current formulation.

SCALING AND DISCRETIZATION

Scaling is important to ensuring good and consistent convergence in all cases. The dynamics of the system are scaled to keep the values near one and to keep any variable from having extra emphasis due to its magnitude. Originally, the problem was run without scaling and the optimizer had difficulties finding a feasible solution. All distance parameters are scaled by R_0, velocity by v_{sc}, acceleration by g_0, time by t_{sc} and angular rate by ω_{sc}. These scale factors are seen in Eq. (67).

$$R_0 = \gamma\,, \quad g_0 = \tfrac{\mu}{R_0^2}\,, \quad v_{sc} = \sqrt{R_0 g_0}\,, \quad t_{sc} = \sqrt{\tfrac{R_0}{g_0}}\,, \quad \omega_{sc} = \sqrt{\tfrac{g_0}{R_0}} \tag{67}$$

The distance scale factor is set to the *smallest* semi-major axis value (γ). This choice is consequential, because it keeps the scaled radius to no smaller than unity, which in turn will prevent the terms such as $1/r^3$ and $1/r^5$ in the gravitational acceleration from becoming very large values. When the largest semi-major axis was used, the iterations failed to converge on a single answer. Instead the iterations bounced between two trajectories. The mass variable (q) is not scaled as the natural log function acts as a scaling function and keeps q near one.

The linear equations of motion are in continuous time; however, optimizers require the problem to be in discrete time. A simple discretization and propagation with the trapezoidal rule was applied. The problem

is divided into n number of time points with a fixed dt time step between each point. The trapezoidal rule is used to propagate the trajectory between the points as demonstrated in Eq. (68).

$$\vec{x}_j = \vec{x}_{j-1} + 0.5dt\left(A_j\vec{x}_j + A_{j-1}\vec{x}_{j-1} + B_j\vec{u}_j + B_{j-1}\vec{u}_{j-1} + c_j + c_{j-1}\right) \tag{68}$$

Each of the n-1 points is represented this way, with j being the current point and j-1 the previous point. The first point j = 1 is the initial vehicle condition. The problem can be rearranged (Eq. (69)), so that it is a function of the previous point and the coefficient matrices.

$$\vec{x}_j = \left[I - 0.5dtA_j\right]^{-1}\left[\left(I + 0.5dtA_{j-1}\right)\vec{x}_{j-1} + 0.5dt\left(B_j\vec{u}_j + B_{j-1}\vec{u}_{j-1} + c_j + c_{j-1}\right)\right] \tag{69}$$

I is the identity matrix. A, B, and c are evaluated based on the previous iteration, prior to solving the optimization problem. This form replaces the continuous dynamics in Problem P3 as n-1 additional equality constraints levied on the problem. An advantage of formulating the equations in this manner is that the optimizer does not require a propagator.

In the analysis a time step of 2.0 seconds was used. This was compared to smaller time steps of 1.0 second and 0.5 second, with negligible change in the results. The smaller time steps increase the number of equality constraints levied on the problem, thus increasing the number of calculations and the run time of the simulation. Care should be taken to balance the accuracy from the propagation and the number of equality constraints.

ANALYSIS AND RESULTS

The entire problem was coded in Matlab to examine feasibility, convergence and descent trajectory trends. The convex optimizer chosen as the testbed was CVX.[19] CVX is a publicly available Matlab based solver for disciplined convex problems. The discrete version of Problem P3 is in a form accepted by CVX. Iterations were considered completed when the position vector between the previous and current iteration was less than 3 cm apart at any trajectory point.

The sample spacecraft used in the analysis consisted of 1000 kg dry mass with 400 kg of propellant. The trajectories used a small fraction of the usable propellant, so this can be thought of as having more dry mass and payload on the vehicle. The maximum thrust was 80 N and the minimum thrust was 20 N with a 225 second Isp.

Three sizes of a generic triaxial asteroid were investigated, A1: 1000 x 500 x 250 m, A2: 750 x 500 x 250 m and A3: 500 x 500 x 250 m. Each asteroid rotates around the largest moment of inertia (+z axis) with a constant spin rate, which is reasonable as the majority of asteroids rotate around their largest moment of inertia.[17] The gravitational coefficients for the 2x2 triaxial spherical model can be analytically calculated and are given in Eq. (70).[17]

$$\begin{aligned} C_{2,0} &= \frac{1}{5r_o^2}\left(\gamma^2 - \frac{\alpha^2+\beta^2}{2}\right) \\ C_{2,2} &= \frac{1}{20r_o^2}\left(\alpha^2 - \beta^2\right) \end{aligned} \tag{70}$$

The size of the asteroid determines these coefficients with α corresponding to the largest semi-major axis, β to the intermediate semi-major axis and γ to the smallest semi-major axis. In addition, four different spin rates were examined. These are described by the amount of time it takes for the asteroid to complete one revolution. The periods are 12 hours, 8 hours, 4 hours and 2 hours. The analysis focused on the 8 hr period with the A1 asteroid. The additional cases were confirmation of trends.

Table 1. Spacecraft initial conditions.

	r_{0_x} (m)	r_{0_y} (m)	r_{0_z} (m)	v_{0_x} (m/s)	v_{0_y} (m/s)	v_{0_z} (m/s)
NP	-50	-50	1000+γ	2	1	0
EQ	1000+α	-50	-50	0	2	1

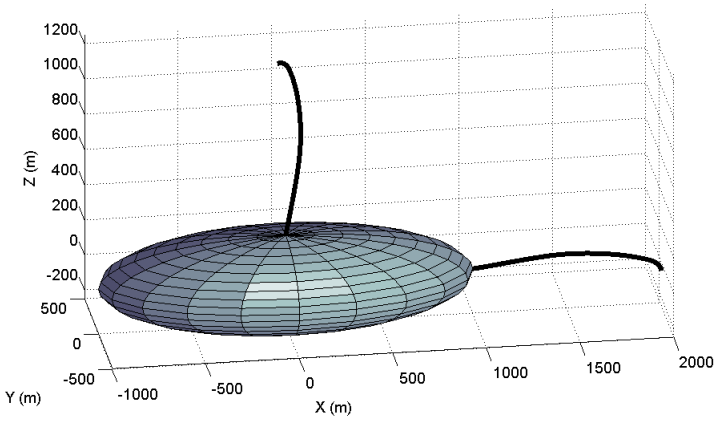

Figure 3. Vehicle trajectory for NP (top) and EQ (right) for a 380 second flight time.

Four trajectories were analyzed during the investigation to ensure that the methodology is robust. The first two cases start 1000 m in altitude, uprange and out of plane from the landing site, along with an initial velocity needing to be slowed. One landing site is on the +z axis or the north pole of the asteroid (NP) with an equatorial trajectory landing on the +x axis (EQ). Figure 3 shows these two trajectories for a 380 second flight time. The initial spacecraft state is located in Table 1. The second set of cases hover 1000 m above the landing site and rotate with the landing site. There is both a north pole (NP_hov) and an equatorial (EQ_hov) hovering case. An additional challenge for the equatorial cases is the landing site rotation inducing a small velocity relative to the ACF frame. The north pole trajectories do not have this challenge. Its challenge is a stronger gravitational acceleration and a steep change in the gravitational acceleration approaching the surface.

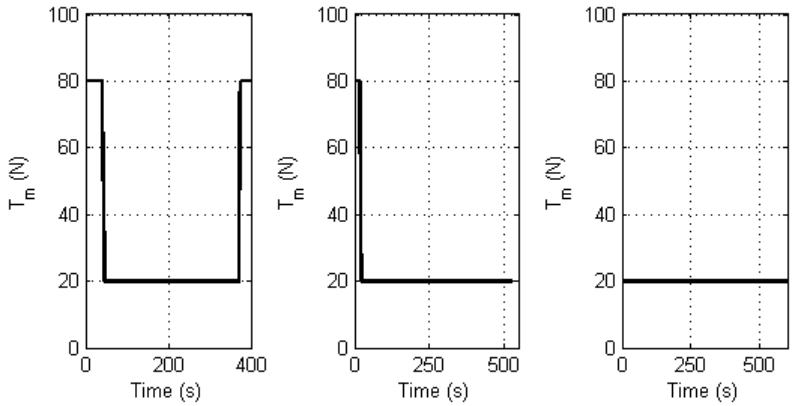

Figure 4. Thrust profiles for EQ 400 s (left), 525 s (middle), 600 s, (right) flight time, showing the three different classes of thrust profiles.

The thrust magnitude follows the traditional bang-bang profile common in optimal control problems. Overall there are three profiles that are prevalent, maximum-minimum-maximum, maximum-minimum and minimum. Shorter flight times have the maximum-minimum-maximum profiles and long flight times have minimum thrust for the entire flight. The maximum-minimum occurs in between the two. Figure 4 contains an example of each of these three classes of thrust profiles.

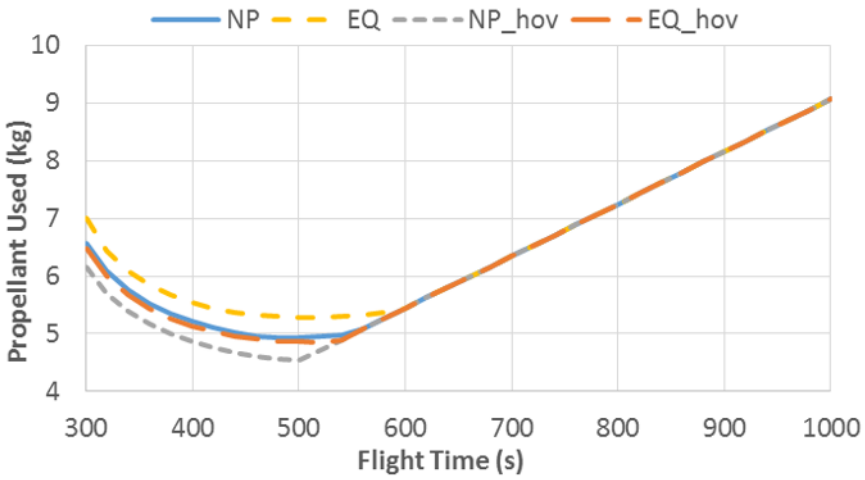

Figure 5. Propellant used as a function of flight time for 1000 x 500 x 250 m with an 8 hr period.

Table 2. Flight times corresponding to events .

(s)	NP	EQ	NP_hov	EQ_hov
min prop	488	512	501	525
start max-min	465	521	474	529
start all min	553	598	502	536

Table 3. Percent difference in mass from minimum propellant case.

	NP	EQ	NP_hov	EQ_hov
start max-min	0.33%	0.019%	0.45%	0.002%
start all min	1.8%	2.5%	0.17%	0.19%

Parameter sweeps changing the length of flight were performed for all the trajectories, asteroids and periods. The parameter sweeps for the four trajectories landing on the 1000 x 500 x 250 m asteroid with an 8 hr period are shown in Figure 5. The propellant used is a convex function in the form of a quadratic spliced with a linear function. The point where the splice occurs (slope changes) and all periods use the same amount of propellant is where the thrust profile switches to minimum thrust for the entire trajectory. After this point the length of flight overwhelms the trajectory, gravity, asteroid size and period aspects in determining propellant usage. Table 2 lists the time that the switch from maximum-minimum-maximum to maximum-minimum occurs corresponding to this parameter sweep, along with the switch to all minimum thrust.

Ideally, the spacecraft would fly the trajectory pertaining to the minimum propellant used over all flight times (optimal flight time). Table 2 lists the optimal flight time in the first row. This minimum propellant

trajectory occurs before the switch to all minimum thrust trajectories. For the EQ trajectory the minimum propellant case occurs before the switch to maximum-minimum, while it occurs after this switch for the other three trajectories. The propellent usage is flat near the minimum propellant trajectory, especially before the minimum propellant case. There is less than a 1% change in propellant used if the burn is 30 seconds shorter than the optimal flight time. After the burn, the propellant usage increases faster than before due to the proximity of the switch to the all minimum thrust on the hover cases. However, it remains less than a 2% change within 10 seconds after the minimum propellant case. The switch to maximum-minimum occurs within 0.5% difference of the minimum propellant case as seen in Table 3.

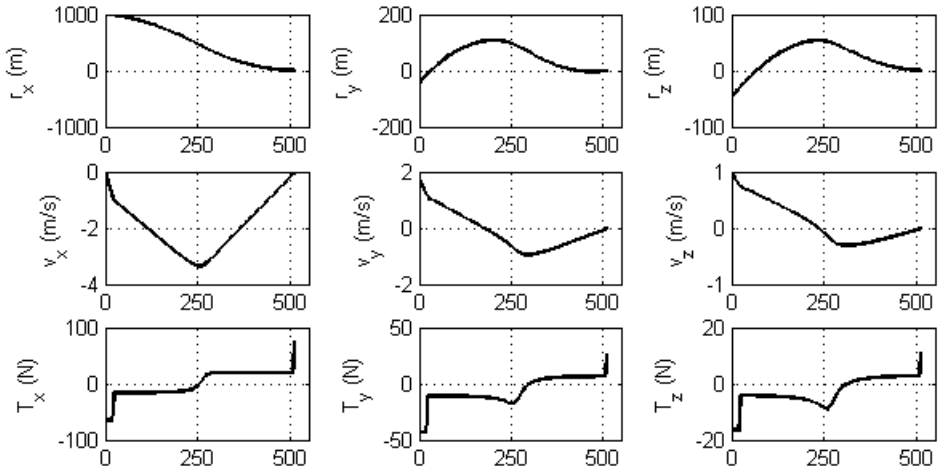

Figure 6. EQ trajectory 512 s flight time, for 1000 x 500 x 250 m with 8 hr period. Spacecraft position (top row) and velocity (middle row) relative to landing site. Thrust profile bottom row.

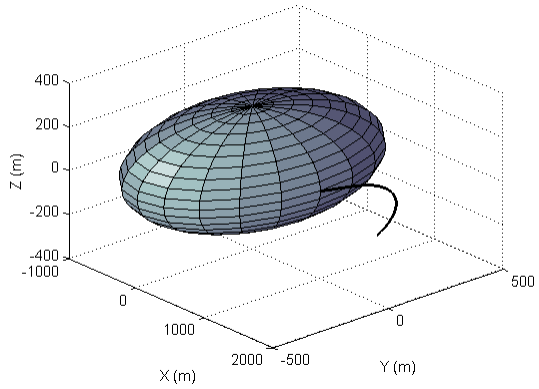

Figure 7. EQ 3-D position for 512 second flight time, for 1000 x 500 x 250 m with 8 hr period.

A look at the fully designed trajectory for the minimum propellant EQ case for the 8 hr period 1000 x 500 x 250 m can be found in Figure 6. The position and velocity are plotted with respect to landing site. The position path that the spacecraft will follow down to the surface is shown in Figure 7. This trajectory has zero velocity relative to the asteroid surface upon touchdown as was designed in the optimization problem.

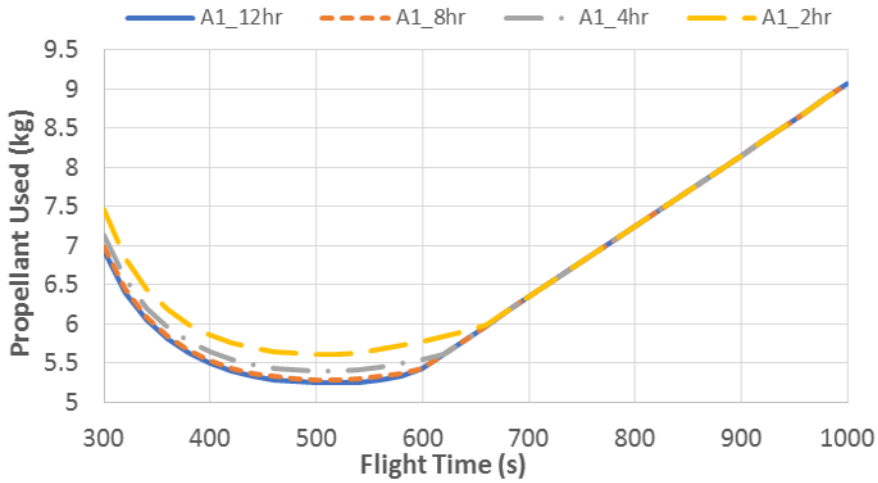

Figure 8. Propellant used as a function of flight time for EQ 1000 x 500 x 250 m asteroid for all four periods.

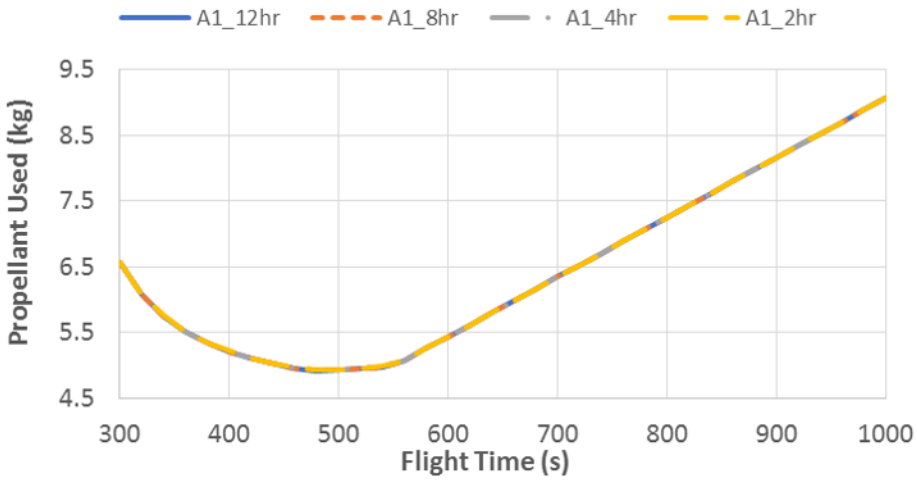

Figure 9. Propellant used as a function of flight time for NP 1000 x 500 x 250 m asteroid for all four periods.

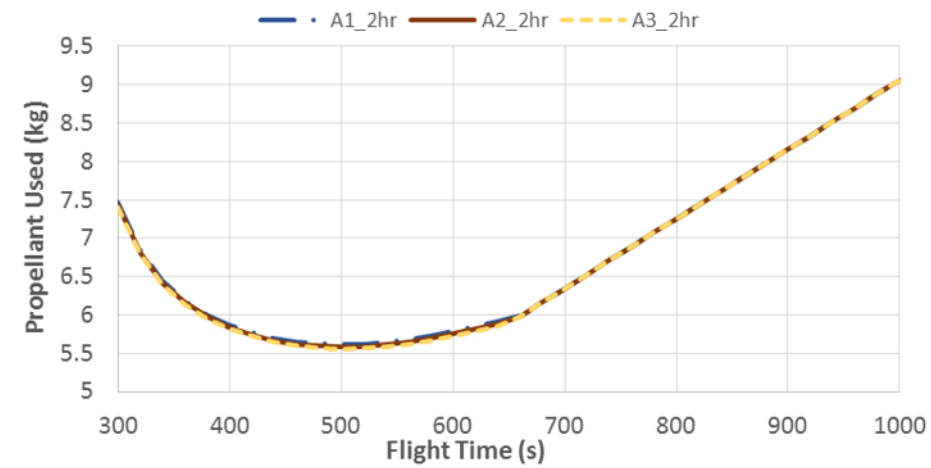

Figure 10. Propellant used as a function of flight time for EQ 2 hour flight period for the three asteroid sizes.

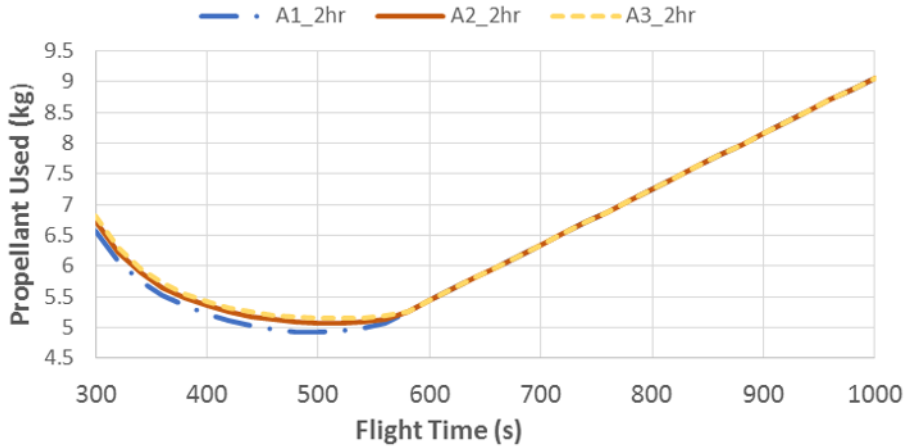

Figure 11. Propellant used as a function of flight time for NP 2 hour flight period for the three asteroid sizes.

The trajectory design worked great for the three asteroid sizes and the four rotation periods for all four trajectories. The equatorial trajectories are sensitive to the rotation rate, with more propellant needed for the faster rotation (2 hours). Figure 8 shows EQ flight time parameter sweeps for the four revolution periods with the 1000 x 500 x 250 m asteroid. The other two asteroid sizes showed the same trends, as well as the EQ_hov trajectories. The north pole trajectories are not affected by the revolution speed of the asteroid, as the north pole landing site is on the rotation axis. Figure 9 confirms this, showing the parameter sweep for the 1000 x 500 x 250 m asteroid for all four periods. Examining the trends for asteroid size, shows that the equatorial trajectories are not sensitive to the asteroid size, while the north pole trajectories are. Figure 10 depicts the EQ parameter sweep for a 2 hr period for the three asteroids, with very little difference between the three. The 8 hr period had no difference between the asteroids. Figure 11 contains the NP parameter sweep for a 2 hr period for the three asteroids. As the asteroid decreases in size, the propellant usage increases. The hover trajectories showed identical trends to the non-hover trajectories.

A good measure of how rapidly this methodology can work is how many iterations (successive solution

problems) were required to design the trajectory. Overall, between 2 to 5 iterations were required, with the majority being 3 or 4 iterations. Unlike propellant used, there were no trends among asteroid size, rotation speed or flight time that drove the number of iterations. The equatorial cases tended to have more trajectories that took 2 iterations and fewer 5 iterations. To give an idea of the simulation run time, a 600 second case with four iterations took 3.5 minutes, with each iteration solving for approximately 3300 variables. This code has not been scrubbed for efficiency, nor written in the most efficient language. It is expected that this time will decrease significantly, when programmed for efficiency. Also, in-depth analysis could reduce the number of nodes.

CONCLUSION

This paper demonstrates that the minimum fuel powered descent problem can be turned into a convex optimization problem, while still retaining the same optimal solution as the original problem. Successive solution method is the key to handling the nonlinear gravity model and adds the flexibility of switching to higher fidelity gravity models in the future. The algorithm successfully handled a wide range of trajectories fleshing out its ability to be adaptable to the asteroid parameters after the asteroid has been characterized upon spacecraft arrival. Trajectories landing near the asteroid's equator are sensitive to the rotation speed, while trajectories landing near the poles will be sensitive to the asteroid size in terms of propellant required for landing. Propellant used for flight times near the minimum propellant case differ very little from the optimal case. Therefore, the exact flight time of the minimum propellant case does not need to be known with a high degree of accuracy. Overall, this is a viable algorithm for rapidly designing powered descent trajectories autonomously on-board the spacecraft.

REFERENCES

[1] David Dunham et. al., "Implementation of the First Asteroid Landing," *Icarus*, Vol 159, 2002, pp. 433-438.

[2] Tetsuo Yoshimitsu, Jun'ichiro Kawaguchi, Tatsuaki Hashimoto, Takashi Kubota, Masashi Uo, Hideo Morita, and Kenichi Shirakawa, "Hayabusa-final autonomous descent and landing based on target marker tracking," *Acta Astronautica*, Vol 65, 2009, pp. 657-665.

[3] J. Bernard, F. Dufour, P. Gaudon, T. Ceolin and S. Kerambrun, "Rosetta Mission Analysis of the Landing Phase on a Comet," *AIAA/AAS Astrodynamics Specialist Conference and Exhibit*, August 2002.

[4] Stephan Ulamec and Jens Biele, "Surface elements and landing strategies for small bodies missions - Philae and beyond," *Advances in Space Research*, Vol 44, 2009, pp. 847-858.

[5] L. Richter, et. al., "Marco Polo Surface Scout (MASCOT) - Study of an Asteroid Lander for the Marco Polo Mission," *60th International Astronautical Congress*, October 2009, pp. 1331-1344.

[6] C. Dietze, et. al. "Landing and Mobility Concept for the Small Asteroid Lander MASCOT on Asteroid 1993 JU3," *61st International Astronautical Congress*, 2010, pp. 9266-9278.

[7] Kevin Berry, Brain Sutter, Alex May, Ken Williams, Brent Barbee, Mark Beckman and Bobby Williams, "OSIRIS-REx Touch-And-Go (TAG) Mission Design and Analysis," *Advances in the Astronautical Sciences*, v. 149, 2013, pp 667-678.

[8] Paolo Lunghi, Michele Lavagna and Roberto Armellin, "A semi-analytical guidance algorithm for autonomous landing," *Advances in Space Research*, Vol 55, No. 11, June 2015, pp. 2719 -2738.

[9] G. Lantoine and R. D. Braun, "Optimal Trajectories for Soft Landing on Asteroids," *Advances in the Astronautical Sciences*, Vol 129 part 1, 2008, pp. 447-468.

[10] Roberto Furfaro, Dario Cersosimo and Daniel Wibben, "Asteroid Precision Landing via Multiple Sliding Surfaces Guidance Techniques," *Journal of Guidance, Control and Dynamics*, Vol 36, No 4, July-August 2013, pp. 1075-1092.

[11] Qixun Lan, Shihua Li, Jun Yang and Lei Guo, "Finite-time soft landing on asteroids using nonsingular terminal sliding mode control," *Transactions of the Institute of Measurement and Control*, Vol 36(2), 2014, pp. 216-223.

[12] Hongwei Yang, Yang Chen and Hexi Baoyin, "Fuel optimal guidance for soft landing on irregular asteroids using sliding mode control," *64th International Astronautical Congress*, 2013, pp. 4949-4960.

[13] Behcet Acikmese and Scott Ploen, "Convex Programming Approach to Powered Descent Guidance for Mars Landing," *Journal of Guidance, Control, and Dynamics*, Vol 30, No 5, Sept-Oct 2007, pp. 1353-1366.

[14] Behcet Acikmese, John Carson and Lars Blackmore, "Lossless Convexification of Nonconvex Control Bound and Pointing Constraints of the Soft Landing Optimal Control Problem," *IEEE Transactions on Control Systems Technology*, Vol 21, No 6, November 2013, pp. 2104 - 2113.

[15] Ping Lu and Xinfu Liu, "Autonomous Trajectory Planning for Rendezvous and Proximity Operations by Conic Optimization," *Journal of Guidance, Control, and Dynamics*, Vol 36, No 2, March-April 2013, pp. 375-389.

[16] David Vallado, *Fundamentals of Astrodynamics and Applications*. 4th ed , CA: Microcosm Press, 2013.

[17] Daniel Scheeres, *Orbital Motion in Strongly Perturbed Environments*, NY: Springer, 2014.

[18] L. S. Pontryagin, V. G. Boltyanskii, Q. V. Gramkreledze and E.F. Mishchenko, *The Mathematical Theory of Optimal Processes*, NY: Intersciences, 1962.

[19] Michael Grant and Stephen Boyd, *CVX: Matlab software for disciplined convex programming*, version 2.0, April 2011. http://cvxr.com/cvx

[20] Stephen Boyd and Lieven Vandenberghe, *Convex Optimization*, NY: Cambridge University Press, 2004.